JOURNAL OF VIROLOGY, June 1998, p. 4918–4924 Vol. 72, No. 6
0022-538X/98/$04.00+0

Transmissible Gastroenteritis Coronavirus Induces Programmed Cell Death in Infected Cells through a Caspase-Dependent Pathway

JEAN-FRANÇOIS ELEOUET,* STEFAN CHILMONCZYK, LYDIA BESNARDEAU, AND HUBERT LAUDE

Unité de Virologie et Immunologie Moléculaires, Institut National de la Recherche Agronomique, 78350 Jouy-en-Josas, France

Received 15 October 1997/Accepted 16 March 1998

In this report, we show that apoptosis (or programmed cell death) is induced in different cell lines infected with a coronavirus, the porcine transmissible gastroenteritis virus (TGEV). Kinetic analysis of internucleosomal DNA cleavage by agarose gel electrophoresis and flow cytometry or cytometric monitoring of the mitochondrial transmembrane potential showed that, for ST cells infected with TGEV, the first overt signs of apoptosis appeared from 10 to 12 h postinfection on. They preceded morphological changes characteristic of cells undergoing apoptosis, as observed by light and electron microscopy. The tripeptide pan-ICE (caspase) inhibitor *N*-benzyloxycarbonyl-Val-Ala-Asp-fluoromethylketone blocked TGEV-induced apoptosis with no effect on virus production. The thiol agent pyrrolidine dithiocarbamate inhibited apoptosis, suggesting that TGEV infection may lead to apoptosis via cellular oxidative stress. The effect of TGEV infection on activation of NF-κB, a transcription factor known to be activated by oxidative stress, was examined. NF-κB DNA binding was shown to be strongly and quickly induced by TGEV infection. However, transcription factor decoy experiments showed that NF-κB activation is not critical for TGEV-induced apoptosis.

The *Coronaviridae* family is a group of enveloped viruses with a large, positive-stranded RNA genome of about 30 kb which comprises two genera, *Coronavirus* and *Torovirus*. This family has been recently grouped in the new order *Nidovirales* together with the *Arteriviridae* family (reviewed in reference 7a). Coronaviruses cause a wide spectrum of diseases in humans and animals but primarily infect the respiratory and gastrointestinal mucosa (reviewed in reference 38). These infections are generally acute, and destruction of the lining epithelia is considered to be a central event in their pathogenesis. When propagated in culture, coronaviruses generally induce extensive cell death. However, the nature of the events leading to cell death in coronavirus-infected cells remains largely unknown.

In recent years, a number of viruses have been shown to induce programmed cell death (PCD), an active cellular self-destruction process that plays an essential role in development and homeostasis but also in cell defense against viral infections (for reviews, see references 35, 37, 43, and 46). The molecular pathways used by viruses to induce apoptosis are still poorly understood. For influenza virus, it has been proposed that the double-stranded-RNA-activated protein kinase could play a role in the induction of apoptosis (42). For a dozen viruses, a viral gene product has been identified as an apoptosis-inducing factor (reviewed in reference 43), but for RNA viruses (excluding retroviruses) only open reading frame 5 (p25) of the arterivirus porcine reproductive and respiratory syndrome virus (41), glycoprotein E^{rns} of pestiviruses (4), and structural capsid protein VP2 of infectious bursal disease virus (10) were shown to induce apoptosis when expressed alone in a cell culture. On the other hand, as endonucleases are activated during apoptosis, many DNA viruses have evolved genes encoding proteins which suppress or delay apoptosis, thus allowing production of large amounts of progeny virus. For example, the poxvirus *crmA* gene product (44) and baculovirus p35 (6) prevent induction of apoptosis by inhibition of the cell death central effector machinery, which includes the cysteine proteases (caspases) of the ICE/CED-3 family that are activated during apoptosis (reviewed in reference 29).

The role of apoptosis in the pathogenesis of coronavirus infections is poorly documented. T-cell-mediated apoptosis in murine hepatitis virus-infected cells has been observed in vivo (21). T-cell depletion mediated by apoptosis was recently evidenced in feline infectious peritonitis virus-infected, diseased cats and shown to involve noninfected cells (12). Direct apoptosis in virus-infected cells could not be detected in vitro in either of these studies. We sought to address this issue by using transmissible gastroenteritis virus (TGEV) as a model. TGEV, a porcine coronavirus, replicates in the differentiated enterocytes covering the intestinal villi, inducing a severe atrophy which results in acute diarrhea (33). TGEV can be propagated ex vivo in a variety of porcine cell lines, including swine testis (ST) cells (27) and various cell lines expressing porcine aminopeptidase N (APN), which acts as a cellular receptor for TGEV (7). The infected monolayers undergo obvious cytopathic changes characterized by shrinking of the cells, which detach from the plate. In this paper, we demonstrate that TGEV induces PCD ex vivo in different cell lines by morphologic, cytometric, and biochemical means. Apoptosis was found to be blocked by the caspase inhibitor *N*-benzyloxycarbonyl-Val-Ala-Asp-fluoromethylketone (Z-VAD.fmk) and inhibited by pyrrolidine dithiocarbamate (PDTC), a thiol reducing agent. The transcription factor NF-κB was activated strongly and early in TGEV-infected cells but did not appear to be a major effector of TGEV-induced apoptosis.

MATERIALS AND METHODS

Viruses and antiapoptotic drugs. The American high cell passage Purdue-115 strain of TGEV and French isolate RM4 of porcine respiratory coronavirus (PRCV) were used as virus sources and propagated on ST and swine kidney (strains PDH and RPTG [rein de porc Thiverval-Grignon]) cells as described previously (19). For TGEV UV inactivation, 25 ml of a virus inoculum was placed into a petri dish (10-cm diameter) on ice and exposed to a 254-nm wavelength lamp (1.368 mW/cm^2) for 6 min. The thiol reducing agent PDTC was added to the medium immediately after infection to a final concentration of 100

* Corresponding author. Mailing address: INRA, Unité de Virologie et Immunologie Moléculaires, 78352 Jouy-en-Josas cedex, France. Phone: (33) 1 34 65 26 41. Fax: (33) 1 34 65 26 21. E-mail: eleouet@biotec.jouy.inra.fr.

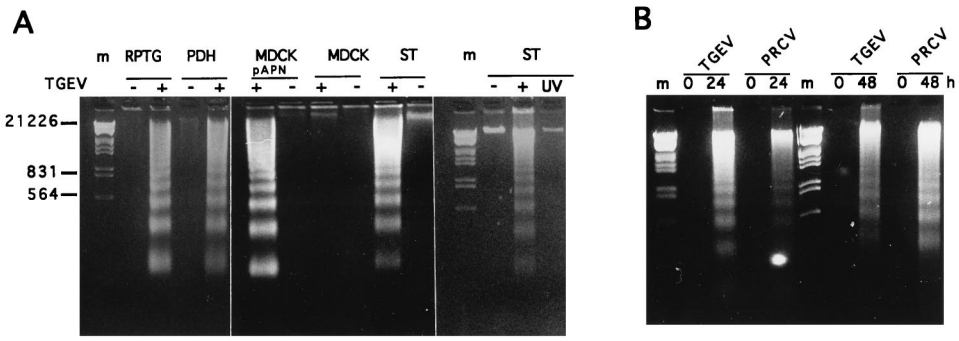

FIG. 1. DNA fragmentation analysis of cells infected with TGEV and PRCV. (A) Low-molecular-weight DNA was isolated at 18 h p.i. from virus-infected (+; MOI, ≈5) or mock-infected (−) cells of the indicated lines. Lane UV contained DNA from cells inoculated with a UV-irradiated TGEV inoculum. (B) DNA was isolated from ST cells at 24 and 48 h p.i. with TGEV or PRCV. Samples were electrophoresed in 2% agarose gels ($5 \cdot 10^5$ cell equivalents per lane) and visualized with ethidium bromide. DNA marker band sizes (lane m) are indicated in bases.

μM. Because PDTC is expected to rapidly lose its activity during incubation (32), the concentration was readjusted every 8 h. For caspase inhibition experiments, the following drugs (from Bachem, Bubendorf, Switzerland) were employed: the interleukin 1β-converting enzyme inhibitor tetrapeptide acetyl-Tyr-Val-Ala-Asp-chloromethylketone (Ac-YVAD-cmk), the apopain inhibitor acetyl-Asp-Glu-Val-L-aspartic acid aldehyde (Ac-DEVD-CHO), and the ICE-like protease inhibitor tripeptide Z-VAD.fmk. Ac-DEVD-CHO was dissolved in H_2O; the two other caspase inhibitors were dissolved in dimethyl sulfoxide with a final concentration in cultures of <0.1% (vol/vol). Two hours before infection, these synthetic modified peptides were added to the medium at a concentration of 100 μM and maintained at that concentration after infection. Control cells received 0.1% dimethyl sulfoxide, which had no effect on cell proliferation or viability.

DNA fragmentation assay. Low-molecular-weight DNA was extracted from approximately 10^6 cells as described by Hinshaw et al. (14), with slight modifications. Briefly, infected or uninfected cells detaching from the plate were centrifuged at 200 × *g* and pooled with the trypsinized adhering cells for each of the time point tested. Cells were washed in phosphate-buffered saline (PBS), resuspended in 500 μl of ice-cold lysis buffer (10 mM Tris [pH 7.5], 10 mM EDTA, 0.2% Triton X-100), and incubated on ice for 30 min. Lysates were centrifuged at 10,000 × *g* at 4°C for 10 min, and supernatants were extracted once with buffered phenol, once with buffered phenol-chloroform, and once with chloroform-isoamyl alcohol (24:1, vol/vol). DNA was ethanol precipitated with 500 mM NaCl. DNA samples were resuspended in 15 μl of sterile water and treated for 15 min at 37°C with RNase A at a final concentration of 0.5 μg/μl, and half of the sample was run on a 2% agarose gel in 1× Tris-borate-EDTA buffer and stained with ethidium bromide.

Flow cytometry. (i) Cell nucleus DNA content. For each plate, detached cells and trypsinized adherent cells were pooled, centrifuged, fixed in 70% ethanol for 1 h, washed in PBS, incubated for 15 min at 37°C with 100 μM RNase A, and stained with propidium iodide as described by Nicoletti et al. (30).

(ii) $\Delta\Psi_m$. Cells were trypsinized, washed twice in PBS, and incubated with 40 nM 3,3′-dihexyloxacarbocyanine iodide [$DIOC_6(3)$; Molecular Probes] in PBS for 15 min at 37°C. Cells treated with the mitochondrial transmembrane potential ($\Delta\Psi_m$)-disrupting protonophore carbonyl cyanide *m*-chlorophenylhydrazone (100 μM, 15 min) served as a negative control. Flow cytometry was done with a Becton Dickinson cytofluorometer. Data analysis was performed with Lysis II software (Becton Dickinson).

Fluorescence and electron microscopy. Apoptotic nuclei were visualized by using cells fixed and stained as described above. Observations were performed on a UV light microscope. For electron microscopy, ST cells were pelleted by centrifugation, washed twice with PBS, fixed with 1.25% glutaraldehyde buffered with sodium cacodylate (0.1 M, pH 7.3), and then postfixed in 2% osmium tetroxide. After dehydration, samples were embedded in Epon araldite. Thin (70-nm) sections were stained with lead citrate and uranyl acetate and then examined with a Philips EM12 electron microscope operated at 80 kV.

EMSAs and supershift analysis. For electrophoretic mobility shift assays (EMSAs), ST cells mock infected or infected with TGEV at a multiplicity of infection (MOI) of 5 were lysed in Totex buffer (31). A ^{32}P-labeled oligonucleotide (35 fmol) with a κB consensus sequence (5′-AGTTGAGGGGACTTTCC CAGGC-3′) was used as a probe and incubated for 20 min at room temperature with a total extract containing 4 μg of protein. Competition was performed by using an excess of unlabeled NF-κB or an unrelated SP1 probe (5′-ATTCGAT CGGGGCGGGGCGAGC-3′). DNA-protein complexes were run on a 4% polyacrylamide gel. Supershifts were performed with antibodies to NF-κB subunits p65 (murine) and p50 (human), kindly provided by Alain Israel, Institut Pasteur, Paris, France. The antibody (1 μl) was added to the binding mixture 20 min after the radiolabeled NF-κB probe. The reaction mixture was incubated for 20 min, and the complexes were resolved as described above.

Transcription factor decoy experiments. Phosphorothioated oligonucleotides were kindly provided by P. Marianneau and P. Després, Institut Pasteur, Paris, France. These modified NF-κB oligonucleotides, used as transcription factor decoys (TFDs), contained three copies of the κB consensus sequence (26). TFDs were added to the cell medium to a concentration of 3 μM 24 h before infection and maintained at that concentration in the medium until the cells were lysed.

RESULTS

TGEV induces internucleosomal DNA cleavage in different cell lines. To investigate whether apoptotic cell death was triggered by TGEV, virus-infected cells were first examined for the presence of a DNA ladder. For each cell line, an extensive cytopathic effect (CPE) was observed at around 16 h postinfection (p.i.) when an MOI of 5 was used, i.e., the cells rounded and detached from the plate. Internucleosomal DNA cleavage was analyzed at 18 h p.i. in three porcine cell lines, ST, PDH, and RPTG, and in MDCK-APN, a clone of a canine kidney cell line expressing porcine APN, which is a receptor for TGEV (7). A DNA ladder was observed for the four cell lines after infection (Fig. 1A). This was not the case for MDCK cells not expressing porcine APN, which are fully refractory to TGEV infection. Neither a CPE nor DNA ladder formation was observed when a UV-inactivated inoculum was used as a control. PRCV, a respiratory variant of TGEV (reviewed in reference 20), was also capable of inducing DNA fragmentation (Fig. 1B), with delayed kinetics, consistent with a replication rate slower than that of TGEV.

TGEV induces apoptotic morphological changes in infected cells. TGEV-infected cells were examined by optical microscopy after fixation with ethanol and staining with propidium iodide, a fluorescent DNA intercalator (30). Most of the infected ST cells showed a marked nuclear diameter reduction and obvious chromatin condensation 18 h after infection (Fig. 2B). TGEV-infected and mock-infected cells fixed at 12 and 24 h p.i. were used for analysis of ultrastructural alterations. Morphological changes typical of the late stage of apoptosis were only observed with cells fixed at 24 h p.i. At that stage, only nucleolar remnants could be found in the convoluted nuclei, which contained small masses of condensed chromatin (Fig. 2D). Mitochondria appeared swollen, indicating that they were no longer functional.

Kinetic analysis of TGEV-induced apoptosis. Further experiments were carried out to establish the time course of nuclear DNA degradation relative to that of cell death. As shown in Fig. 3A, internucleosomal DNA cleavage was detected by 12 h p.i. Nuclear DNA degradation was also monitored by flow cytometry analysis of cells fixed and stained with propidium

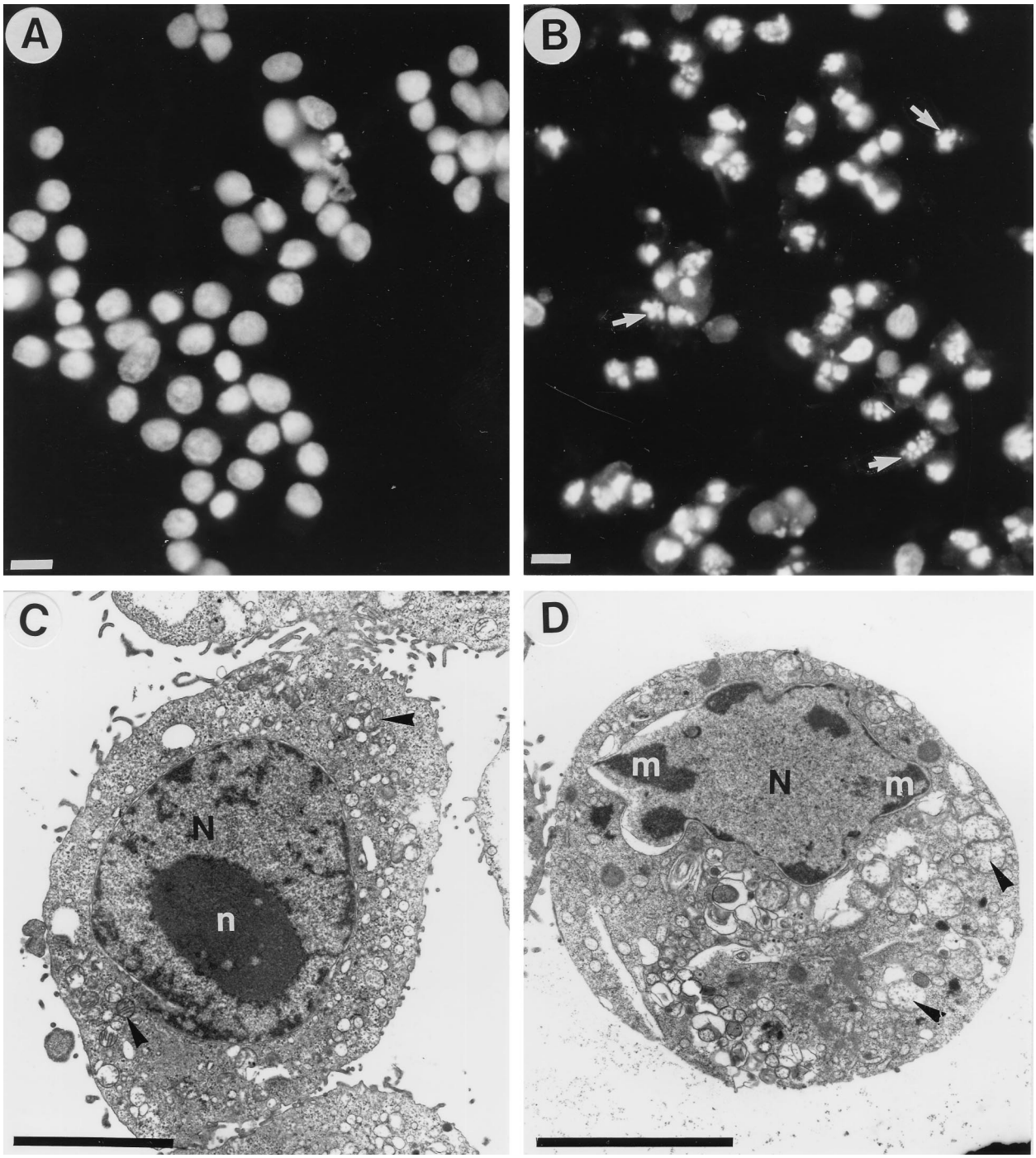

FIG. 2. Morphological changes in virus-infected cells. (A and B) Fluorescence microscopic appearance of ethanol-fixed, propidium iodide-stained, and mock-infected (A) or TGEV-infected (B) ST cells. At 18 h p.i., most of the infected cells (arrows) show apoptotic bodies due to the condensation of chromatin in several micronuclei (bars, 20 μm). (C and D) Electron micrographs of mock-infected (C) and TGEV-infected (D) ST cells at 24 h p.i. In a mock-infected cell (C), the round nucleus (N) displays a large, unique, electron-dense nucleolus (n). Mitochondria (arrowheads) are dispersed within the cytoplasm. A TGEV-infected cell (D) is characterized by numerous masses of condensed chromatin (m) dispersed at the periphery of a convoluted nucleus (N) and swollen mitochondria (arrowheads) (bars, 5 μm).

iodide. With this technique, a lower fluorescence signal is emitted by apoptotic cells compared to normal cells, corresponding to a lower nuclear DNA content (see references 30 and 35). Results from a typical experiment are shown in Fig. 3B. Apoptotic nuclei appeared as a broad, subdiploid DNA (A_0) peak easily distinguished from the narrow peak of cells with normal (diploid) DNA content in the red fluorescence. The proportions of subdiploid DNA-containing nuclei in samples were 20, 60, and 70% at 12, 18, and 24 h p.i., respectively. This result shows that the majority (>70%) of cells entered apoptosis following TGEV infection. A usual feature of apoptotic cells is that loss of membrane integrity occurs in the final stages of the

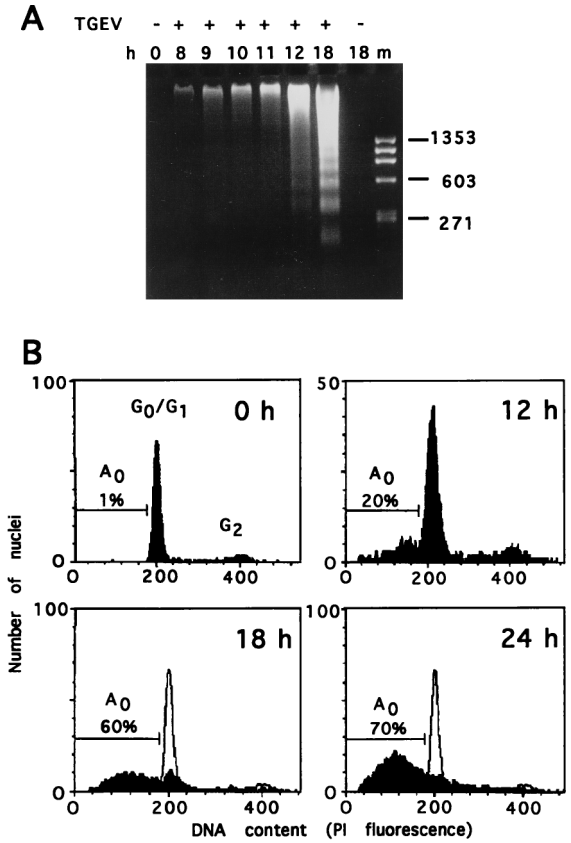

FIG. 3. Time course of TGEV-induced DNA fragmentation in ST cells. (A) At the indicated times after infection, DNA was isolated from virus- or mock-infected cells and analyzed as described in the legend to Fig. 1. Lane m contained DNA size markers (sizes are in bases). (B) Flow cytometric DNA fluorescence profiles of TGEV-infected ST cells at different times p.i. The percentages of cells with subdiploid ($<G_0/G_1$) A_0 DNA content are indicated. PI, propidium iodide.

process. When ST cells were tested for the ability to exclude the vital dye trypan blue, the percentages of blue cells were only 6, 25, and 40% ± 5% at 18, 24, and 48 h p.i., respectively. Taken together, these results supported the view that PCD is an important component of TGEV-induced cell death.

Accumulating data indicate a breakdown of mitochondrial function during apoptosis (reviewed in references 34 and 39). Cytofluorometric analysis of $\Delta\Psi_m$ was performed for TGEV-infected ST cells with the potential-sensitive dye $DIOC_6(3)$. As shown in Fig. 4, a $\Delta\Psi_m$ transition, indicating a loss of mitochondrial function, occurred between 10 and 12 h p.i. and progressed until 24 h p.i.

TGEV-induced apoptosis is blocked by the caspase inhibitor Z-VAD.fmk. The central effector machinery of PCD is composed of cytoplasmic proteases called caspases. These are present in an inactive form and are irreversibly activated during the effector phase of apoptosis, leading to ultrastructural alterations, chromatin condensation, and nuclear fragmentation. In humans, 10 caspases have been identified and some of them can be blocked by specific synthetic peptides (reviewed in references 13 and 29). To determine whether TGEV-induced apoptosis involves caspase activation, experiments were performed with the irreversible tetrapeptide ICE (caspase 1) subfamily protease inhibitor Ac-YVAD.cmk, the reversible tetrapeptide apopain (caspase 3) inhibitor Ac-DEVD-CHO, and the irreversible tripeptide pan-ICE inhibitor Z-VAD.fmk (40, 48). These inhibitors were used at a concentration of 100 μM,

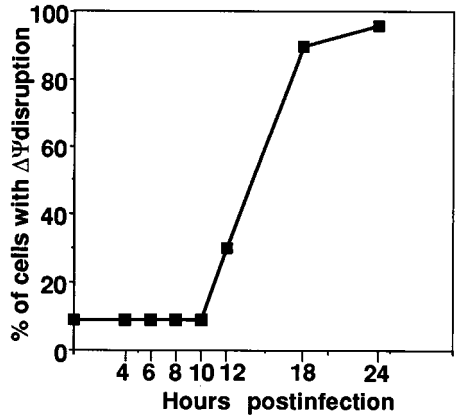

FIG. 4. Kinetics of mitochondrial failure. Membrane potential $DIOC_6(3)$ fluorescence was analyzed by flow cytometry. The percentage of ST cells presenting a drop in fluorescence was measured at different times p.i., as indicated.

which has been shown to allow complete protease inhibition in cultured mammalian cells after induction of apoptosis by various molecules (8, 9, 16, 28). Incubation of cells with Z-VAD.fmk prior to infection with TGEV completely blocked the appearance of apoptotic nuclei and the onset of nuclear DNA fragmentation until at least 48 h p.i. (Fig. 5A). Importantly, virus production in Z-VAD.fmk-treated cells was similar to that in untreated cells (Fig. 5B). Apparently, the Z-VAD.fmk treatment had no clear effect on the maintenance of cell membrane integrity, as assessed by trypan blue staining. However, there was a dramatic change in the appearance of infected cells (Fig. 6). No protection against TGEV-induced apoptosis was observed when Ac-YVAD.cmk or Ac-DEVD-CHO was used, possibly due to a low permeability of the cells to these drugs (data not shown). Similar results have been obtained with leukemic cell death induced by interleukin-3 withdrawal, against which DEVD.fmk and Ac-YVAD.cmk did not protect, in contrast to Z-VAD.fmk (3).

TGEV-induced apoptosis is inhibited by the thiol agent PDTC. Direct exposure of various cell types to oxidants such as

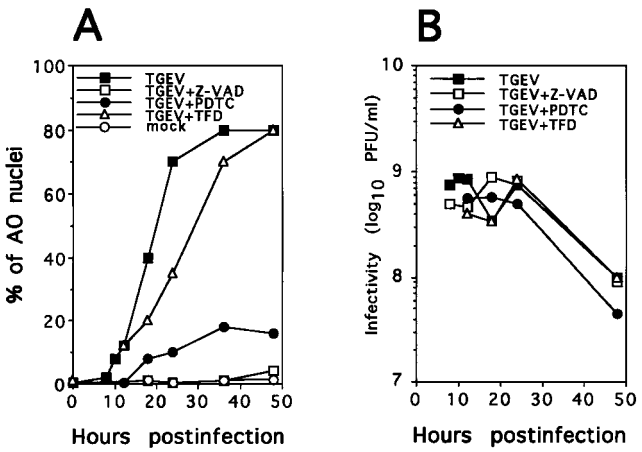

FIG. 5. Effects of Z-VAD.fmk, PDTC, and an NF-κB decoy on nuclear apoptosis and virus production in TGEV-infected ST cells at an MOI of 5. (A) At the indicated times p.i., the percentage of cells with apoptotic nuclei was determined by flow cytometry as described in the legend to Fig. 2. Mock-infected cells treated with TFD gave the same percentage of A_0 nuclei, and the measured values are superimposed on those of untreated, mock-infected cells. (B) Effects of different drugs on TGEV replication. At the indicated times, the virus titer was determined by plaque assay.

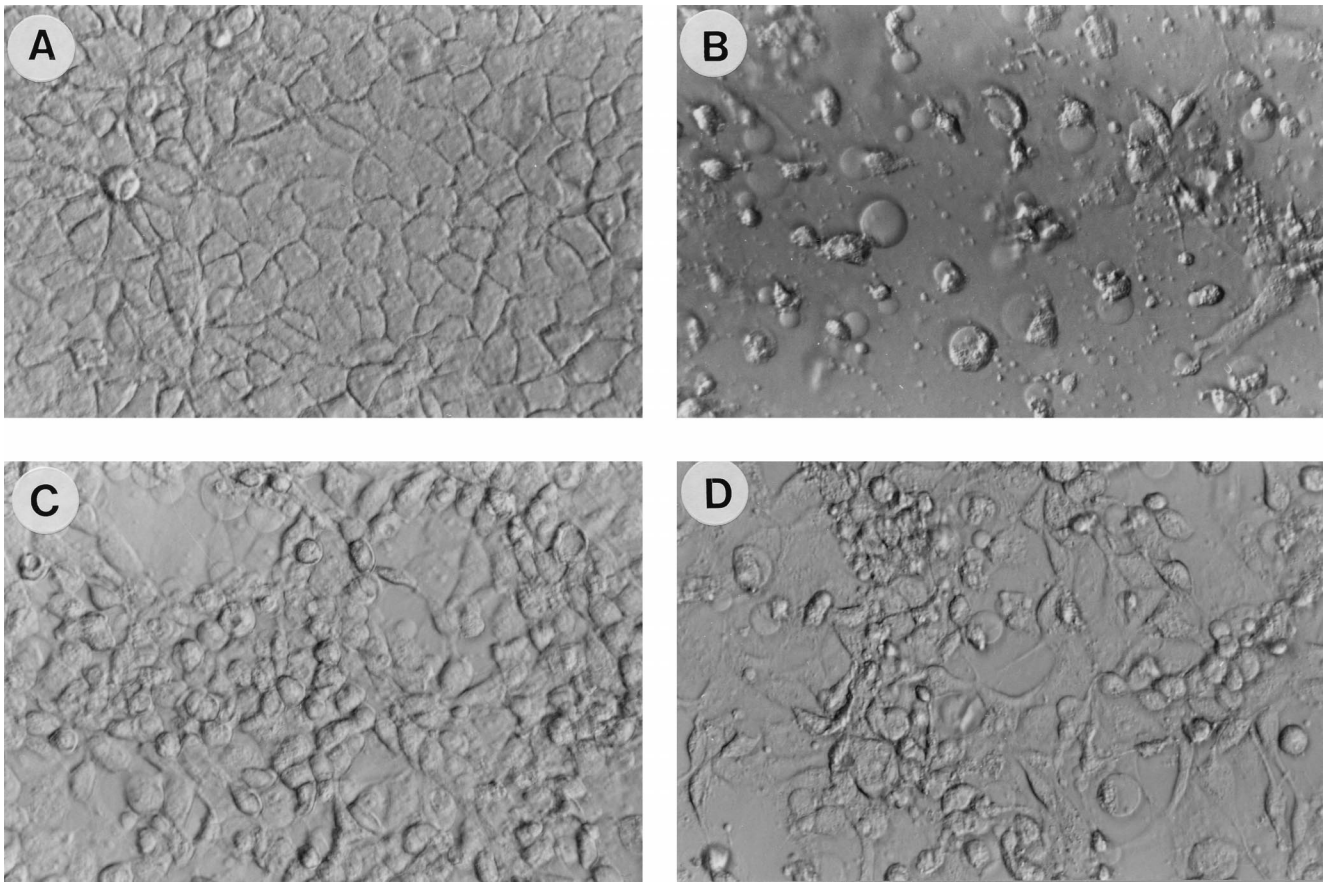

FIG. 6. Effect of Z-VAD.fmk or PDTC treatment on the CPE of TGEV on ST cells at an MOI of 5 PFU/cell. Phase-contrast images of mock-infected (A) and TGEV-infected (B) ST cells in the presence of 100 μM Z-VAD.fmk (C) or PDTC (D) were taken at 28 h p.i. at an original magnification of ×400. The appearance of uninfected, PDTC- or Z-VAD.fmk-treated cells was identical to that of untreated cells.

hydrogen peroxide or lipid hydroperoxides can directly induce apoptosis, while in many experimental models, pretreatment of cells with antioxidants has been shown to protect against this form of cell death. For example, the thiol reducing agent PDTC has been shown to prevent alphavirus-induced apoptosis (24). To investigate whether such agents could prevent apoptosis in TGEV-infected cells, various concentrations of PDTC were added to the medium at the beginning of infection. A nearly complete protective effect of PDTC against TGEV-induced apoptosis at concentrations as low as 50 μM was observed at 18 h p.i., as shown by a DNA ladder assay (data not shown). Flow cytometry analysis of DNA degradation showed that TGEV-induced apoptosis was markedly inhibited by PDTC (Fig. 5B), with no change in cumulative virus production compared to that in untreated cells (Fig. 5B). PDTC also had a protective effect against the CPE (Fig. 6) and cellular membrane damage, with only 15% ± 5% of trypan blue-positive cells at 48 h p.i. These results suggest that an abnormal cellular oxidation event may occur during TGEV infection, which might account for cell injury and PCD induction.

NF-κB is activated in TGEV-infected cells. PDTC is a very effective inhibitor of the activation of NF-κB (36), a family of dimeric transcription factors (reviewed in reference 2). NF-κB activation can induce or inhibit apoptosis, and this probably depends on its subunit composition and cell type and the nature of the apoptotic stimulus. To investigate whether TGEV infection induces NF-κB activation, total cell lysates were prepared at various times p.i. and DNA-protein complexes were analyzed by EMSAs. Strong and quick NF-κB DNA-binding activity was induced during infection by TGEV, whereas only background activity was detected in noninfected cells (Fig. 7A and B). NF-κB DNA-binding activity began to increase as early as 3 h p.i. and reached a maximum at 9 h p.i. To identify the NF-κB subunits detected by EMSA in infected ST cells, subunit-specific antibodies to human p50 and murine p65 were added during in vitro DNA binding. A strong band corresponding to the complex supershifted was observed with both anti-p50 and anti-p65 antibodies (Fig. 7C). These results suggest that the activated NF-κB complex detected may involve p65 and p50 subunits, even if the presence of other NF-κB subunits cannot be excluded.

To determine whether the activation of NF-κB could be responsible for the induction of PCD in TGEV-infected ST cells, NF-κB decoy experiments were performed with a probe containing human NF-κB binding sites. Treatment of cells with TFD completely inhibited the NF-κB binding activity induced by TGEV (Fig. 7D). Fluorocytometry analysis showed that nuclear DNA degradation kinetics were slightly slower in TFD-treated cells than in untreated cells (Fig. 5A). No effect on cell viability was observed after TFD treatment of uninfected control cells until after 11 h p.i. However, virus production was also slightly retarded (virus titer fourfold lower at 12 h p.i.; Fig. 5B). From these results, it was concluded that the

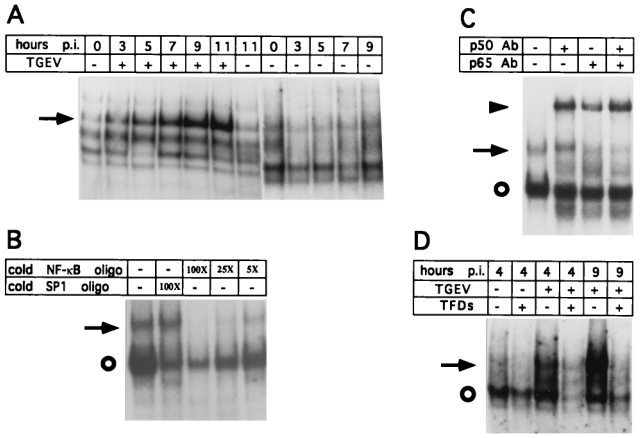

FIG. 7. Activation of NF-κB in TGEV-infected ST cells. (A) EMSAs were performed with a total extract containing 4 μg of protein by using a ^{32}P-labeled oligonucleotide with a consensus κB sequence (see Materials and Methods). The arrow indicates the NF-κB-specific complex. (B) The specificity of the retarded complexes was assessed by preincubating an extract with an excess of an unlabeled (cold) NF-κB or an unrelated SP1 oligonucleotide (oligo) probe, as indicated. The slower-migrating band indicated by the arrow disappeared completely when an unlabeled NF-κB competitor was included, indicating that this complex is specific for the NF-κB probe. The faster-migrating band indicated by the circle was partially competed by unlabeled NF-κB or an unrelated SP1 probe, indicating that it is not specific for the NF-κB probe. (C) Analysis of the subunit composition of the major complex induced by TGEV infection. Specific antibodies (Ab) to human p50 and murine p65 were added to the total binding mixture as described in Materials and Methods. The arrow indicates the NF-κB complex. Supershifted complexes are indicated by the arrowhead. (D) Inhibition of NF-κB binding activity by NF-κB decoy experiments. Double-stranded phosphorothioate oligonucleotides used as TFDs contain three copies of the consensus κB sequence (26). TFDs were added to the cell medium to a concentration of 3 μM 24 h before TGEV infection. At 4 and 9 h p.i., total cell lysates were prepared and subjected to EMSAs as described for panel A. The arrow points to the major NF-κB retarded complex induced by TGEV infection. Note that the faster-migrating band indicated by the circle was poorly affected by the TFDs, confirming that it is not specific for the NF-κB probe.

NF-κB activation observed in TGEV-infected ST cells plays a secondary role, if any, in the induction of PCD.

DISCUSSION

This report provides clear evidence that TGEV induces apoptotic cell death, as shown by internucleosomal DNA cleavage, nuclear condensation, and breakdown of $\Delta\Psi_m$ in ST cells. Signs of apoptosis were observed in three other TGEV-infected cell lines, including a nonporcine cell line stably expressing porcine APN as a virus receptor. The first signs of apoptosis could be observed at around 12 h p.i., concomitant with the end of the viral cycle (18). TGEV-induced apoptosis was shown to be caspase dependent, based on the preventive effect of Z-VAD.fmk, an inhibitor of proapoptotic ICE-like proteases (caspases). Inhibition of TGEV-induced apoptosis with Z-VAD.fmk did not enhance or inhibit virus production as measured at 18 h p.i. These observations are consistent with the notion that apoptosis could play a crucial role in the CPE of TGEV. Recently, Sindbis virus (SV)-induced apoptosis was shown to be inhibited by Z-VAD.fmk (28a). Treatment of human immunodeficiency virus-infected T cells by caspase inhibitors has been shown to sustain virus production (5). It has been suggested that Z-VAD.fmk inhibits apoptosis by blocking a key effector protease upstream of at least four other caspases (25). It would be interesting to define more precisely the nature of the caspases activated during TGEV-induced apoptosis.

Although the morphological features of apoptosis have been appreciated for several decades, the biochemical pathways responsible for induction of apoptosis are only beginning to be elucidated. In this study, we investigated different biochemical aspects of TGEV-induced apoptosis in an attempt to understand by which pathway cell death is triggered during infection. The production of reactive oxygen species has been proposed to be an important, although facultative, pathway for induction of PCD (17). Activation of the transcription factor NF-κB is necessary for SV-induced apoptosis in rat AT-3 prostate carcinoma cells, and it was proposed that the inhibitory effect of several antioxidants, including PDTC, against SV (AR339)-induced apoptosis in rat AT-3 prostate carcinoma cells was due to their ability to inhibit NF-κB activation (24). This mechanism was also proposed for dengue virus, for which virus-induced apoptosis was blocked by NF-κB decoy experiments (26). Two of our observations suggest that oxidative stress may occur during TGEV infection: (i) the thiol agent PDTC was shown to inhibit the apoptotic process, and (ii) NF-κB was activated a few hours after the virus cycle had started. However, this transcription factor did not seem to be necessary for induction of apoptosis, as shown by NF-κB decoy experiments. This suggests that for TGEV, pathways activated by oxidative stress, possibly via functional impairment of the endoplasmic reticulum (1, 31), but not involving NF-κB activation, may account for virus-induced apoptosis.

Recent data suggest that mitochondria are well placed to be sensors of oxidation damage and may play a major role in PCD (reviewed in references 11 and 47). Nuclear apoptosis can be preceded by a precipitous collapse of $\Delta\Psi_m$ and loss of selective ion permeability, leading to the formation of mitochondrial permeability transition pores and the release of apoptosis-initiating factors, triggering the latent activity of caspases. Cells with a low $\Delta\Psi_m$ rapidly proceed to DNA fragmentation, within 15 min to several hours (17). Time course analysis of TGEV-infected ST cells showed a breakdown of $\Delta\Psi_m$ roughly concomitant with the beginning of internucleosomal DNA cleavage. More precise kinetics, however, would be required to determine whether mitochondrial breakdown precedes the activation of caspases and DNA degradation.

It has been proposed that Bcl-2, a natural antiapoptotic factor present essentially in mitochondrial membranes, neutralizes the damaging effects of oxidants (15). Bcl-2 is believed to prevent apoptosis by regulating the mitochondrial pore permeability transition and by inhibiting caspases via an intermediate (17a). Overexpression of human Bcl-2 was first shown to block or delay apoptosis induced by infection with SV and influenza viruses (14, 22). Similar results have been observed with other, but not all, viruses (23, 45). Preliminary experiments indicated that human Bcl-2 is unable to block or delay apoptosis induced by TGEV infection, suggesting that pathways that cannot be inhibited by Bcl-2 may be activated during TGEV infection.

In conclusion, the present study provided evidence that TGEV can act as a true apoptotic inducer in cultured cells. The available data point to oxidative stress as a possible trigger for TGEV-induced apoptosis. However, owing to the recognized complexity of this biological process, additional investigations are needed to substantiate this view. An important finding is that TGEV-induced cell death could be efficiently prevented by a caspase inhibitor, consistent with the notion that apoptosis potentially represents a major mechanism in the viral CPE. Accordingly, it would be interesting to examine in vivo whether PCD plays a role in the pathogenesis of TGEV infection. Finally, TGEV is, to our knowledge, the first coronavirus reported to trigger direct apoptosis in infected cells. It would be

worth pursuing investigations to determine whether such a property could be shared by other members of this family.

ACKNOWLEDGMENTS

We are grateful to Philippe Després and Philippe Marianneau for constructive comments and the gift of reagents and protocols; Alain Israel (Institut Pasteur, Paris, France) for helpful discussions of NF-κB; Patrice Petit (CNRS, Villejuif, France) for precious help with $\Delta\Psi_m$ determination; Karine Poulard and Céline Reverdy for excellent technical help; Kathi Archbold for revising the English version of the manuscript; Monique Nézondé and Francis Fort for photographs; J. M. Hardwick, David Vaux, and Miha Pakusch for providing the Bcl-2 cDNA; and Virginie Joulin for advice on caspase studies.

REFERENCES

1. **Baeuerle, P. A., and T. Henkel.** 1994. Function and activation of NF-kappa B in the immune system. Annu. Rev. Immunol. **12:**141–179.
2. **Baeuerle, P. A., and D. Baltimore.** 1996. NF-kappa B: ten years after. Cell **87:**13–20.
3. **Barge, R. M., R. Willemze, P. Vandenabeele, W. Fiers, and R. Beyaert.** 1997. Differential involvement of caspases in apoptosis of myeloid leukemic cells induced by chemotherapy versus growth factor withdrawal. FEBS Lett. **409:** 207–210.
4. **Bruschke, C. J. M., M. M. Hulst, R. J. M. Moormann, P. A. van Rijn, and J. T. van Oirschot.** 1997. Glycoprotein E^{ms} of pestiviruses induces apoptosis in lymphocytes of several species. J. Virol. **71:**6692–6696.
5. **Chinnaiyan, A. M., C. Woffendin, V. M. Dixit, and G. J. Nabel.** 1997. The inhibition of pro-apoptotic ICE-like proteases enhances HIV replication. Nat. Med. **3:**333–337.
6. **Clem, R. J., M. Feichheimer, and L. K. Miller.** 1991. Prevention of apoptosis by a baculovirus gene during infection of insect cells. Science **254:**1388–1390.
7. **Delmas, B., J. Gelfi, R. l'Haridon, L. K. Vogel, H. Sjöstrom, O. Norén, and H. Laude.** 1992. Aminopeptidase N is a major receptor for the enteropathogenic coronavirus TGEV. Nature **357:**417–419.

7a. **de Vries, A. A. F., M. C. Horzinek, P. J. M. Rottier, and R. J. de Groot.** 1997. The genome organization of the Nidovirales: similarities and differences between arteri-, toro-, and coronaviruses. Semin. Virol. **8:**33–47.

8. **Dubrez, L., I. Savoy, A. Hammam, and E. Solari.** 1996. Pivotal role of a DEVD-sensitive step in etoposide-induced and Fas-mediated apoptotic pathways. EMBO J. **15:**5504–5512.
9. **Enari, M., H. Hug, and S. Nagata.** 1995. Involvement of an ICE-like protease in Fas-mediated apoptosis. Nature **375:**78–81.
10. **Fernàndez-Arias, A., S. Martìnez, and J. F. Rodrìguez.** 1997. The major antigenic protein of infectious bursal disease virus, VP2, is an apoptotic inducer. J. Virol. **71:**8014–8018.
11. **Golstein, P.** 1997. Controlling cell death. Science **275:**1081–1082.
12. **Haagmans, B. L., H. F. Egberink, and M. C. Horzinek.** 1996. Apoptosis and T-cell depletion during feline infectious peritonitis. J. Virol. **70:**8977–8983.
13. **Henkart, P. A.** 1996. ICE family proteases: mediators of all apoptotic cell death? Immunity **4:**195–201.
14. **Hinshaw, V. S., C. W. Olsen, N. Dybdahl-Sissoko, and D. Evans.** 1994. Apoptosis: a mechanism of killing by influenza A and B viruses. J. Virol. **68:**3667–3673.
15. **Hockenbery, D. M., Z. N. Oltvai, X.-M. Yin, C. L. Milliman, and S. J. Korsmeyer.** 1993. Bcl-2 functions in an antioxidant pathway to prevent apoptosis. Cell **75:**241–251.
16. **Jacobsen, M. D., M. Weil, and M. C. Raff.** 1996. Role of Ced-3/ICE-family proteases in staurosporine-induced programmed cell death. J. Cell. Biol. **133:**1041–1051.
17. **Kroemer, G., N. Zamzami, and S. A. Susin.** 1997. Mitochondrial control of apoptosis. Immunol. Today **18:**45–51.

17a. **Kroemer, G.** 1997. The proto-oncogene Bcl-2 and its role in regulating apoptosis. Nat. Med. **3:**614–620.

18. **Laude, H., J. Gelfi, and J. M. Aynaud.** 1981. *In vitro* properties of low- and high-passaged strains of transmissible gastroenteritis coronavirus of swine. Am. J. Vet. Res. **42:**447–449.
19. **Laude, H., J.-M. Chapsal, J. Gelfi, S. Labiau, and J. Grosclaude.** 1986. Antigenic structure of transmissible gastroenteritis virus. I. Properties of monoclonal antibodies directed against virion proteins. J. Gen. Virol. **67:** 119–130.
20. **Laude, H., K. Van Reeth, and M. Pensaert.** 1993. Porcine respiratory coronavirus: molecular features and virus-host interactions. Vet. Res. **24:**125–150.
21. **Lee, S. K., H. Y. Youn, A. Hasegawa, H. Nakayama, and N. Goto.** 1994. Apoptotic changes in the thymus of mice infected with mouse hepatitis virus, MHV-2. J. Vet. Med. Sci. **56:**879–882.
22. **Levine, B., Q. Huang, J. T. Isaacs, J. C. Reed, D. E. Griffin, and J. M. Hardwick.** 1993. Conversion of lytic to persistent alphavirus infection by the bcl-2 cellular oncogene. Nature **361:**739–742.
23. **Liao, C. L., Y. L. Lin, J. J. Wang, Y. L. Huang, C. T. Yeh, S. H. Ma, and L. K. Chen.** 1997. Effect of enforced expression of human bcl-2 on Japanese encephalitis virus-induced apoptosis in cultured cells. J. Virol. **71:**5963–5971.
24. **Lin, K. I., S. H. Lee, R. Narayanan, J. M. Baraban, J. M. Hardwick, and R. R. Ratan.** 1995. Thiol agents and Bcl-2 identify an alphavirus-induced apoptotic pathway that requires activation of the transcription factor NF-kappa B. J. Cell Biol. **131:**1149–1161.
25. **MacFarlane, M., K. Cain, X. M. Sun, E. S. Alnemri, and G. M. Cohen.** 1997. Processing/activation of at least four interleukin-1beta converting enzyme-like proteases occurs during the execution phase of apoptosis in human monocytic tumor cells. J. Cell Biol. **137:**469–479.
26. **Marianneau, P., A. Cardona, L. Edelman, V. Deubel, and P. Desprès.** 1997. Dengue virus replication in human hepatoma cells activates NF-κB which in turn induces apoptotic cell death. J. Virol. **71:**3244–3249.
27. **McKlurkin, A. W., and J. O. Norman.** 1966. Studies on transmissible gastroenteritis of swine. II. Selected characteristics of a cytopathogenic virus common to five isolates of transmissible gastroenteritis. Can. J. Comp. Med. Vet. Sci. **30:**190–198.
28. **Muzio, M., A. M. Chinnaiyan, F. C. Kischkel, K. O'Rourke, A. Shevchenko, J. Ni, C. Scaffidi, J. D. Bretz, M. Zhang, R. Gentz, M. Mann, P. H. Krammer, M. E. Peter, and V. M. Dixit.** 1996. FLICE, a novel FADD-homologous ICE/CED-3-like protease, is recruited to the CD95 (Fas/APO-1) death-inducing signaling complex. Cell **85:**817–827.

28a. **Nava, V. E., A. Rosen, M. A. Veliuona, R. J. Clem, B. Levine, and J. M. Hardwick.** 1998. Sindbis virus induces apoptosis through a caspase-dependent, CrmA-sensitive pathway. J. Virol. **72:**452–459.

29. **Nicholson, D. W., and N. A. Thornberry.** 1997. Caspases: killer proteases. Trends Biochem. Sci. **22:**299–306.
30. **Nicoletti, I., G. Migliorat, M. C. Pagliacci, F. Grignani, and C. Riccardi.** 1991. A rapid and simple method for measuring thymocyte apoptosis by propidium iodide staining and flow cytometry. J. Immunol. Methods **139:** 271–279.
31. **Pahl, H., and P. A. Baeuerle.** 1995. A novel signal transduction pathway from the endoplasmic reticulum to the nucleus is mediated by transcription factor NF-κB. EMBO J. **14:**2580–2588.
32. **Pahl, H. L., and P. A. Baeuerle.** 1996. Activation of NF-κB by ER stress requires both Ca^{2+} and reactive oxygen intermediates as messengers. FEBS Lett. **392:**129–136.
33. **Pensaert, M.** 1970. Transmissible gastroenteritis of swine: virus-intestinal cell interactions. II. Electron microscopy of the epithelium in isolated jejunal loops. Arch. Gesamte Virusforsch. **31:**335–351.
34. **Petit, P. X., S. A. Susin, N. Zamzami, B. Mignotte, and G. Kroemer.** 1996. Mitochondria and programmed cell death: back to the future. FEBS Lett. **396:**7–13.
35. **Razvi, E. S., and R. M. Welsh.** 1995. Apoptosis in viral infections. Adv. Virus Res. **45:**1–60.
36. **Schreck, R., P. Rieber, and P. A. Baeuerle.** 1991. Reactive oxygen intermediates as apparently widely used messengers in the activation of the NF-kappa B transcription factor and HIV-1. EMBO J. **10:**2247–2258.
37. **Shen, Y., and T. E. Shenk.** 1995. Viruses and apoptosis. Curr. Opin. Genet. Dev. **5:**105–111.
38. **Siddell, S., H. Wege, and T. Meulen.** 1983. The biology of coronaviruses. J. Gen. Virol. **64:**761–776.
39. **Skulachev, V. P.** 1996. Why are mitochondria involved in apoptosis? Permeability transition pores and apoptosis as selective mechanisms to eliminate superoxide-producing mitochondria and cell. FEBS Lett. **397:**7–10.
40. **Slee, E. A., H. Zhu, S. C. Chow, M. MacFarlane, D. W. Nicholson, and G. M. Cohen.** 1996. Benzyloxycarbonyl-val-ala-asp (Ome) fluoromethylketone (ZVAD.FMK) inhibits apoptosis by blocking the processing of CPP32. Biochem. J. **315:**21–24.
41. **Suarez, P., M. Diaz-Guerra, C. Prieto, M. Esteban, J. M. Castro, A. Nieto, and J. Ortin.** 1996. Open reading frame 5 of porcine reproductive and respiratory syndrome virus as a cause of virus-induced apoptosis. J. Virol. **70:**2876–2882.
42. **Takizawa, T., K. Ohashi, and Y. Nakanishi.** 1996. Possible involvement of double-stranded RNA-activated protein kinase in cell death by influenza virus infection. J. Virol. **70:**8128–8132.
43. **Teodoro, J. G., and P. E. Branton.** 1997. Regulation of apoptosis by viral gene products. J. Virol. **71:**1739–1746.
44. **Tewari, M., and V. M. Dixit.** 1995. Fas- and tumor necrosis factor-induced apoptosis is inhibited by the poxvirus crmA gene product. J. Biol. Chem. **270:**3255–3260.
45. **Ubol, S., P. C. Tucker, D. E. Griffin, and J. M. Hardwick.** 1994. Neurovirulent strains of alphavirus induce apoptosis in bcl-2-expressing cells: role of a single amino acid change in the E2 glycoprotein. Proc. Natl. Acad. Sci. USA **24:**5202–5206.
46. **Vaux, D. L., and A. Strasser.** 1996. The molecular biology of apoptosis. Proc. Natl. Acad. Sci. USA **93:**2239–2244.
47. **Wyllie, A.** 1997. Clues in the p53 murder mystery. Nature **389:**237–238.
48. **Zhu, H., H. O. Fearnhead, and G. M. Cohen.** 1995. An ICE-like protease is a common mediator of apoptosis induced by diverse stimuli in human monocytic THP.1 cells. FEBS Lett. **374:**303–308.